

Online Sampling in the Parameter Space of a Neural Network for GPU-accelerated Motion Planning of Autonomous Vehicles

Mogens Graf Plessen

Abstract—This paper proposes online sampling in the parameter space of a neural network for GPU-accelerated motion planning of autonomous vehicles. Neural networks are used as controller parametrization since they can handle nonlinear non-convex systems and their complexity does not scale with prediction horizon length. Network parametrizations are sampled at each sampling time and then held constant throughout the prediction horizon. Controls still vary over the prediction horizon due to varying feature vectors fed to the network. Full-dimensional vehicles are modeled by polytopes. Under the assumption of obstacle point data, and their extrapolation over a prediction horizon under constant velocity assumption, collision avoidance reduces to linear inequality checks. Steering and longitudinal acceleration controls are determined simultaneously. The proposed method is designed for parallelization and therefore well-suited to benefit from continuing advancements in hardware such as GPUs. Characteristics of proposed method are illustrated in 5 numerical simulation experiments including dynamic obstacle avoidance, waypoint tracking requiring alternating forward and reverse driving with maximal steering, and a reverse parking scenario.

I. INTRODUCTION AND PROBLEM FORMULATION

A. Motivation

This paper is motivated by the desire for a simple control scheme that can (i) be based on arbitrarily complex nonlinear non-convex vehicle models, (ii) work for general all-purpose trajectory planning (i.e., is equally applicable to scenarios from parking to road centerline tracking), (iii) can generate collision-free trajectories accounting for the full vehicle dimensions, and (iv) can exploit continuing advancement in computation hardware, in particular, for parallelization.

B. Problem formulation and contribution

The problem addressed is to design a method to generate control signals (e.g., steering and longitudinal acceleration) such that a full-dimensional vehicle can drive automatically from an initial vehicle state to a desired goal state while avoiding static and dynamic obstacles, and accounting for sensor measurements (perception) and typical environmental constraints (traffic rules). Such a method is visualized abstractly in Fig. 1. This paper focuses on the control aspect, i.e., the design of C. Thus, it is assumed throughout that general high-level route, obstacle points data and other relevant environment measurements are made available by a navigation and perception module not subject of this paper.

The contribution of this paper is a control method that parameterizes controller C in Fig. 1 by a neural network and employs a specific GPU-accelerated gradient-free algorithm for the online sampling of its parameters every

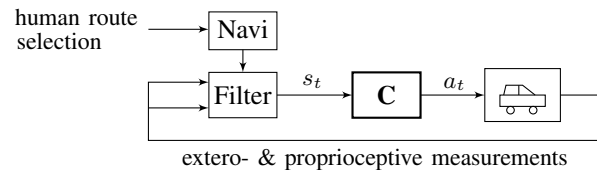


Fig. 1. Closed-loop control architecture. “Navi” and “Filter” map human route selections as well as extero- and proprioceptive measurements to feature vector s_t . This paper proposes a neural network-based and GPU-accelerated online sampling algorithm for controller C, which maps s_t to control action a_t to be applied to the vehicle. The algorithm accounts for physical system constraints and for static and dynamic obstacle avoidance.

sampling time such that all initial motivating aspects (i)-(iv) from Sect. I-A are addressed.

C. Background and further motivation

In the survey of [1] motion planning techniques for automated vehicles are classified into 4 groups: graph-search, sampling, interpolating curve and optimal control based planners. The typical ingredients common to all 4 are: (i) a mathematical vehicle model (possibly nonlinear, non-holonomic and non-convex), (ii) a priori mission information (at least start and goal location; often also high-level map-based route information such as road-centerline references, velocities, etc.), (iii) an exteroceptive and a proprioceptive sensors setup, and (iv) a vehicle’s actuators setup. Then, the 4 groups differ in how they map information (i)-(iii) to control signals fed to (iv) such that the resulting vehicle motion is collision-free. This problem is complex [2]. Therefore, all motion planning techniques typically make additional specific assumptions for their algorithms to work. For example, graph-search and optimal control methods often assume specific obstacle shapes [3]–[7], which necessitates first an upstream mapping of raw sensor data to such obstacle descriptions. In [8], [9] ground robots are approximated as circles to simplify collision checks. Vehicle models employed are of great variety, (i) often differing for tasks (parking, tube-like road driving, limits of handling, etc.), (ii) expressed in different coordinate systems (absolute or road aligned), and (iii) even varying over different hierarchies, for example, when differentiating trajectory generation and consequent tracking [10]. For (i)-(ii), switching logics and multiple controller designs are required. For (iii), hierarchy-encroaching feasibility issues may be encountered.

Sampling based motion planners or, in general, methods that use randomization are attractive since these are *probabilistic complete*: a solution will be found with probability 1 when the simulation effort goes to infinity and a solution exists. Many of such algorithms are founded

on RRTs [11] because of its characteristic expansion of the transition tree heavily biased toward unexplored space. However, randomization comes at a cost. For RRTs, jagged controls, varying costs, varying number of nodes, and varying solution times are typical. This resulted in a large body of work improving the basic RRT-algorithm via heuristics for specific applications [12]–[16]. One issue are “jagged” paths as reported already in the original RRT-paper [11], but also in alternatively popular *search-based* methods [17]. In the latter, a post-processing smoothing step is employed involving both nonlinear optimization plus then interpolation.

The proposed algorithm belongs to the group of sampling based planners. However, its main characteristic is to sample online in the *parameter space* of a neural network parameterizing the controller, an approach not taken in any of the references from the reviews [1], [10] and [18].

After a summary of notation, Sect. II describes the method proposed to solve the problem formulated in Sect. I-B. Numerical simulation experiments are provided in Sect. III. More comments and limitations are summarized in Sect. IV, before concluding in Sect. V.

D. Notation

CoG	Vehicle center of gravity.
EV	Ego-vehicle.
NN	Neural network.
TSHC	Main algorithm from [19].
$(\cdot)_t$	Variable at time-index t .
$n_{(\cdot)} \in \mathbb{N}_{++}$	Variable dimension (e.g., n_z).
$N_{(\cdot)}$	Scalar number of data points.
$H \in \mathbb{N}_{++}$	Prediction horizon.
$\mathcal{M} \in \mathbb{R}^{N_{\mathcal{M}} \times n_{\mathcal{M}}}$	Available a priori mission data.
$N_{\text{restarts}} \in \mathbb{N}_{++}$	Hyperparameter in TSHC [19].
$N_{\text{iter}}^{\text{max}} \in \mathbb{N}_{++}$	Hyperparameter in TSHC [19].
$N_{\text{obstPts}} \in \mathbb{N}_{+}$	Nr. of obstacle points (each 4D).
$P^{\text{min}}/\bar{P}/P^{\text{max}}$	Min/Avg/Max. path length.
$T_s \in \mathbb{R}$	Sampling time.
$\theta \in \mathbb{R}^{1 \times n_{\theta}}$	Vector of NN-parameters.
$a \in \mathbb{R}^{1 \times n_a}$	Control action vector.
$\Delta\xi, \Delta\eta, \Delta\varphi, \Delta v$	Normalization constants in (3).
$\epsilon_{\xi}, \epsilon_{\eta}, \epsilon_{\varphi}, \epsilon_v \in \mathbb{R}$	Tolerances in subscripted states.
$l_f, l_r \in \mathbb{R}$	Distance CoG to front, rear axle.
$m^z \in \mathbb{R}^{1 \times n_{m^z}}$	Proprioceptive measurements.
$m^{\text{ext}} \in \mathbb{R}^{1 \times n_{m^{\text{ext}}}}$	Exteroceptive measurements.
$(m^{\text{ext},x}, m^{\text{ext},y})$	(x, y) -coordinates of m^{ext} .
$\{\hat{m}_{t+h}^{\text{ext}}\}_{h=0}^H$	Extrapolation for prediction.
$m^{\text{ref}} \in \mathbb{R}^{1 \times n_{m^{\text{ref}}}}$	Reference measurements vector.
$n \in \mathbb{N}_{++}$	Hyperparameter in TSHC [19].
$s \in \mathbb{R}^{1 \times n_s}$	Feature vector.
$\bar{\tau}_a \in \mathbb{R}$	Avg. comput. time Step 5 of Alg. 1.
$t \in \mathbb{N}_{+}$	Variable for indexing time: tT_s .
φ, v	Vehicle heading angle and velocity.
(x, y)	Vehicle CoG location.
(ξ, η)	2D EV-aligned coordinate system.
$z \in \mathbb{R}^{1 \times n_z}$	Vehicle state vector.
$\zeta^{\text{goal}} \in \mathbb{R}^{1 \times n_{\zeta^{\text{goal}}}}$	Goal setpoint vector.

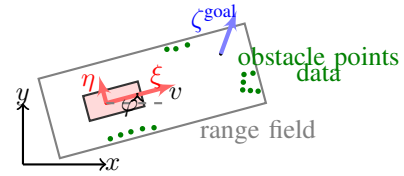


Fig. 2. Visualization of x, y, φ and v , vehicle-aligned coordinates ξ and η , an exemplary setpoint ζ^{goal} and measurable obstacle points data within a range field surrounding an, e.g., rectangular vehicle (red) in the 2D plane.

II. SOLUTION DESCRIPTION

A. Closed-loop algorithm

This paper proposes the closed-loop control architecture visualized in Fig. 1 and Algorithm 1 for closed-loop control of transportation missions in the autonomous vehicles context. The main submodules are discussed below.

Algorithm 1: Closed-loop control algorithm

- 1 **Mission Start:** \mathcal{M} , z_0 and $t = 0$; Sect. II-B.
 - 2 **while** *mission not yet completed* **do**
 - 3 Obtain measurements: $m_t^z, m_t^{\text{ext}}, m_t^{\text{ref}}$; Sect. II-C.
 - 4 Determine goal setpoint: ζ_t^{goal} ; Sect. II-D.
 - 5 Determine control action: a_t ; Sect. II-E.
 - 6 Apply control action a_t to the vehicle.
 - 7 Determine if mission is yet completed.
 - 8 Wait until the next sampling time: $t = t + 1$.
-

B. Step 1: Mission start

A priori *mission data* is summarized by \mathcal{M} , output of a high-level route planner (not subject of this paper). It comprises at least 1 goal setpoint, i.e., the final goal pose described by at least planar location, heading and velocity. It may also describe a reference trajectory, i.e., a sequence of setpoints uniformly or non-uniformly spatially distributed. Ultimately, it may additionally include obstacle information, e.g., map-based information about road-bounds. In general, all data may also be available as sets accounting for uncertainty rather than as point-data only. A transportation mission is completed (Step 7 of Alg. 1) once the final goal setpoint is reached (e.g., a parking position) within a specified tolerance.

The initial vehicle state is denoted by z_0 . It may not necessarily be fully observable. Thus, full state vector information may not be available to the control algorithm.

C. Step 3: Obtaining measurements

According to Fig. 1, it is distinguished between proprio- (m_t^z), exteroceptive (m_t^{ext}), and reference measurements obtained from a high-level route-planner (m_t^{ref}).

Measurements m_t^z can represent any subset of z_t arbitrarily perturbed by noise. In the simplest case, $m_t^z = z_t$.

Measurements m_t^{ext} are assumed to be available (e.g., from lidar and camera sensors) as a set of *obstacle point data* in the EV-aligned coordinate system spanned by ξ - and η -coordinates. Every of the N_{obstPts} obstacle points is assumed as a 4D vector (planar position, heading and velocity). Since vehicles are throughout assumed as ground-contacted systems, projection of all relevant 3D obstacle data to the 2D

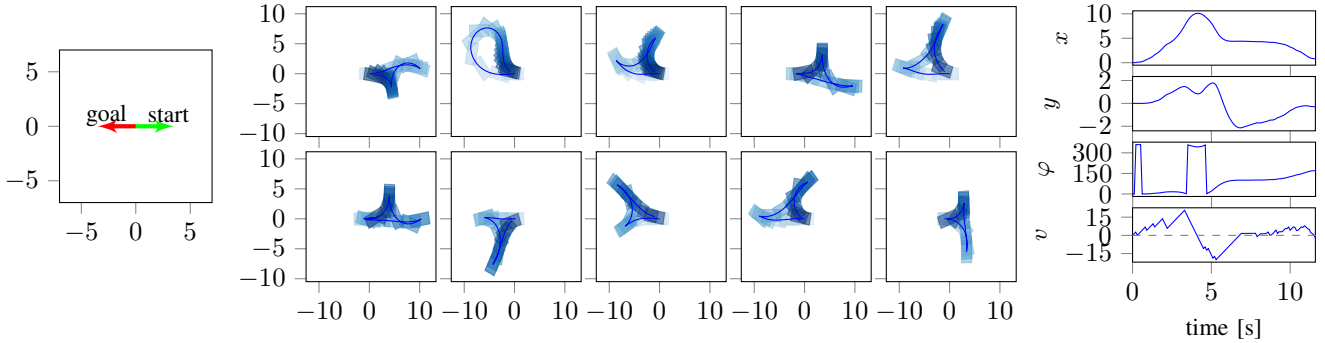


Fig. 3. Experiment 1. (Left) mission formulation: a motion from “start”- to “goal”-pose (both at 0-velocity) is sought. (Center) Planar trajectories for 10 different initial random seeds. In all cases a NN-[5,2,2] is employed. More quantifications are: $\bar{\tau}_a = 0.034\text{s}$, $v^{\min}/\bar{v}/v^{\max} = -29/-1.1/26\text{km/h}$ and $P^{\min}/\bar{P}/P^{\max} = 21.6/26.7/33.4\text{m}$. In 9 out of 10 cases 3-point-steering naturally evolves. (Right) Vehicle states for the grid view at the top-left.

plane permits w.l.o.g. 3D-collision-free trajectory planning. Projections may also account for vehicle height, roll-angle and 3D obstacles.

Reference route data m_t^{ref} may become available as a subset (for finite horizon planning) of preliminary mission data \mathcal{M} indexed spatially along its path. Thus, the first setpoint of m_t^{ref} shall coincide with the reference spatially closest to the absolute (x, y) -coordinates of the EV¹. Alternatively, variable m_t^{ref} is also employed to account for all potentially updated mission data.

D. Step 4: Goal setpoint selection

According to Step 4 of Alg. 1 (intermediate) goal setpoints are set at every sampling time t and described by location, heading and velocity information, i.e.,

$$\zeta_t^{\text{goal}} = [x_t^{\text{goal}} \quad y_t^{\text{goal}} \quad \varphi_t^{\text{goal}} \quad v_t^{\text{goal}}]. \quad (1)$$

Two comments are made. First, the critical importance of ζ_t^{goal} for Alg. 1 is emphasized. The fundamental nature of the proposed method is sampling-based. Therefore, ζ_t^{goal} is selected ideally such that it is reached over the prediction horizon in Step 5 of Alg. 1. However, here no guarantee can be given that it actually will be reached. Efforts undertaken to address this issue heuristically are discussed further in Sect. III, and in Sect. IV discussing limitations of the presented method and outlining ongoing work in this direction.

Second, conceptually the selection of ζ_t^{goal} is to be interpreted as a strategic upstream decision layer *preceding* the control signal generator, which is the main subject of this paper and which is responsible for motion planning of the current vehicle state to ζ_t^{goal} . Considerations for ζ_t^{goal} -design are (i) traffic rules (e.g., setting a traffic light stopping position, a headway position subject to road speed limits, or a leading vehicle for adaptive cruise control as setpoints), and (ii) a recursive logic based on success of reaching ζ_t^{goal} over the prediction horizon at the last sampling time.

E. Step 5: Determining control action

In [19], the TSHC-algorithm is proposed for *offline* encoding of multiple motion primitives in a neural network.

¹In implementation practice, a discrete space-index is used to track the EV’s progress and position along the reference path in case this is available.

For information, a single motion primitive may, e.g., be a left-turn connecting a specific start and goal vehicle pose (described by at least planar position, heading and velocity).

In this paper, the same TSHC-algorithm is also applied, however, for *online* motion planning. Therefore, at every sampling time t only *one* trajectory from the current vehicle state to the designated goal setpoint ζ_t^{goal} is sought online (instead of multiple motion primitives encoded offline as in [19], [20]). By construction, TSHC samples in the parameter space of a neural network that is parameterizing controller C in Fig. 1. The method is suitable for GPU-acceleration. Several comments are made.

First, under the assumption of employing a fixed vehicle model for the EV (e.g., a kinematic or dynamic one) for the forward simulation of the EV-motion over $t, \dots, t+H$, such vehicle model and all its (constant) hyperparameters can be defined directly on the GPU (without the need for passing between host and GPU), since this data is not changing. In contrast, obstacle information at time t must be passed to the GPU, since these measurement data are changing every t . In this paper, the space environment that is prohibited from being trespassed by the EV for collision avoidance is modeled as a set of obstacle points. This data stems from both static and dynamic obstacles. For dynamic motion planning the environment must then be extrapolated over a prediction horizon H , i.e., $\{\hat{m}_{t+h}^{\text{ext}}\}_{h=0}^H$ with $\hat{m}_{t+0}^{\text{ext}} = m_t^{\text{ext}}$. In more detail, in this paper the following is therefore done.

- (i) The obstacle points data vector m_t^{ext} is assumed to contain planar location, heading and velocity information. In practice (and not subject of this paper), only the 2 last relative location positions may be retrieved, based on which heading and velocity must then be estimated, for example, using sensor fusion and model-based estimation techniques such as Kalman filtering.
- (ii) The movement of all obstacle points is extrapolated under the assumptions of *constant velocity* over the prediction horizon H . This is done for a practical reason. Obstacle point locations are extrapolated linearly. In contrast to alternative history-dependent non-linear extrapolation techniques (e.g., constant acceleration with velocity capping), this enables fast collision checks when gridding over all obstacle points at every

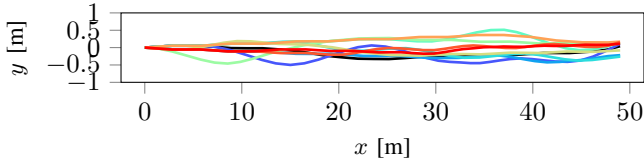


Fig. 4. Experiment 2 for NN-[5,2,2]. Trajectories for 10 different initial random seeds are displayed. Because of the sampling-based nature of the algorithm lateral deviations result. See also Table III.

prediction time $t + h$, $\forall h = 0, \dots, H$.

- (iii) Only m_t^{ext} is passed to the GPU at every t . Extrapolating $\{\hat{m}_{t+h}^{\text{ext}}\}_{h=0}^H$ over the prediction horizon is then implemented directly on the GPU.
- (iv) Extrapolating the movement of obstacle points is done only *once* at time t under the constant velocity assumption, but *not* updated again throughout the simulation horizon $\{t+1, \dots, t+H\}$. In general, when the EV is moving throughout the duration of the simulation horizon, new obstacle points (especially from road bounds) from offline stored maps may become available. However, all of the latter are dismissed. The dismissal is done for computational efficiency. Motion planning can be GPU-accelerated based thereon and without requiring any additional calls to offline stored maps. To further mitigate the relevance of any new obstacle points, the goal setpoint ζ_t^{goal} is always selected *within* or *on* the boundary of the (e.g., rectangular) range field visible at time t .

Second, the employed method for collision-checks (implemented on the GPU) is briefly discussed. In general, the EV can be modeled as an arbitrarily refined polytope (convex or non-convex). Then, a collision with obstacle points boils down to a multidimensional linear inequality check. For example, for typical 2D navigation in the plane it is

$$A(\varphi_{t+h}) \begin{pmatrix} \left[\hat{m}_{t+h}^{\text{ext},x} \right] \\ \left[\hat{m}_{t+h}^{\text{ext},y} \right]_j \end{pmatrix} - \begin{pmatrix} x_{t+h} \\ y_{t+h} \end{pmatrix} < b(\varphi_{t+h}), \quad (2)$$

$\forall h = 0, \dots, H$, $\forall j = 1, \dots, N_{\text{obstPts}}$, and where $A(\varphi_{t+h})$ and $b(\varphi_{t+h})$ are algebraic functions of the vehicle dimensions defining the polygon for the collision check.

Third, due to the sampling-nature of proposed algorithm and typical small sampling times of the closed-loop control system, in general, no guarantee about generating a trajectory actually reaching the goal setpoint can here be given (see Sect. V for ongoing work in this direction). For example, (i) the goal setpoint may be selected as too difficult to be reachable within $t, \dots, t + H$, or (ii) the number of samples is too small (due to computational constraints), or (iii) algorithm hyperparameters may be set unsuitably to generate such trajectory. However, even if not reaching the final goal setpoint, TSHC is designed to at least return a collision-free trajectory. In the extreme case, again due to the sampling nature of the algorithm, no guarantee about finding any collision-free trajectory may be given (e.g., due to a cluttered environment too difficult to navigate in). The larger the number of samples that can be generated by the GPU, the larger the likelihood of generating collision-free trajectories reaching the designated goal setpoint.

l_f	l_r	δ^{max}	$\dot{\delta}^{\text{max}}$	u_v^{min}	u_v^{max}
1.1	1.4	$\frac{40\pi}{180}$	$\frac{20\pi}{180}$	$-\frac{100}{3.8 \times 3.6}$	$\frac{100}{7.4 \times 3.6}$

TABLE I. Constants for the vehicle model. All in SI-units. The vehicle chassis has rectangular dimensions $(l_f + 0.7 + l_r + 0.6) \times 2\text{m}$.

Fourth, for clarity it is summarized what (i) must be passed from host to GPU as part of Step 5 of Alg. 1 at every t , and (ii) what hyperparameters and models can be defined directly on the GPU since being invariant over t . For the former, these are θ , m_t^z , a_{t-1} , ζ_t^{goal} , m_t^{ext} and the current random seed. For the latter, these are the vehicle system model, the controller parametrization structure (here multilayer perceptrons), the method to update σ_{pert} (here randomly as in [20]), and all constant hyperparameters from Table II.

Fifth, θ is initialized at every t for $i_{\text{restart}} = 1, \dots, N_{\text{restarts}}$ as follows:

$$\theta(i_{\text{restart}}) = \begin{cases} \theta_{t-1}^*, & \text{if } i_{\text{restart}} = 1, \\ \theta(i_{\text{restart}} - 1), & \text{if } 2 \leq i_{\text{restart}} \leq N_{\text{restarts}}, \end{cases}$$

where θ_{t-1}^* is the best parametrization that last sampled a trajectory reaching the goal setpoint in prediction.

Sixth, in this paper the feature vector is selected as

$$s_{t+h} = \left[\frac{\xi_t^{\text{goal}} - \xi_{t+h}}{\Delta\xi}, \frac{\eta_t^{\text{goal}} - \eta_{t+h}}{\Delta\eta}, \dots, \frac{\varphi_t^{\text{goal}} - \varphi_{t+h}}{\Delta\varphi}, \frac{v_t^{\text{goal}} - v_{t+h}}{\Delta v}, a_{t-1+h}[0] \right], \quad (3)$$

$\forall h = 0, \dots, H$, and where the first 4 elements denote deviations of the EV w.r.t. ζ_t^{goal} over the prediction horizon in the EV-aligned coordinate system, and where $a_{t-1+h}[0]$ represents the NN-output related to steering control at the subscripted time-instances. All normalization constants are indicated by $\Delta(\cdot)$ to normalize elements for s_t approximately to the range of ± 1 . See Table II for numerical values.

Ultimately, the final control is obtained as the mapping

$$a_t = \mathcal{X}(s_t, \theta^*), \quad (4)$$

where θ^* are the optimal parameters returned by TSHC.

F. Vehicle model

For the simulation experiments in the next section a kinematic 4-states-2-controls vehicle model is used:

$$\begin{bmatrix} \dot{x} \\ \dot{y} \\ \dot{\varphi} \\ \dot{v} \end{bmatrix} = \begin{bmatrix} v \cos(\varphi + \beta) / \cos(\beta) \\ v \sin(\varphi + \beta) / \cos(\beta) \\ v \tan(\delta) / (l_f + l_r) \\ u_v \end{bmatrix}, \quad (5)$$

with $\beta = \text{atan}(l_r \tan(\delta) / (l_f + l_r))$, states $z = [x, y, \varphi, v]$, and controls $\delta = \delta^{\text{max}} a[0]$ and $u_v = u_v^{\text{min}} + \frac{a[1]+1}{2}(u_v^{\text{max}} - u_v^{\text{min}})$. All constants are summarized numerically in Table I.

III. NUMERICAL SIMULATION EXPERIMENTS

All experiments use the same hyperparameters, see Table II. All displayed results are *closed-loop* results at sampling rate 0.1s. Controls are throughout initialized as $a_0 = [0, a_0^{\text{idle}}[1]]$ with $a_0^{\text{idle}}[1] = -1 - 2 \frac{u_v^{\text{min}}}{u_v^{\text{max}} - u_v^{\text{min}}}$, which implicates zero initial acceleration. All simulation experiments were conducted on an Intel i7-7700K CPU@4.20GHz \times 8 and 1

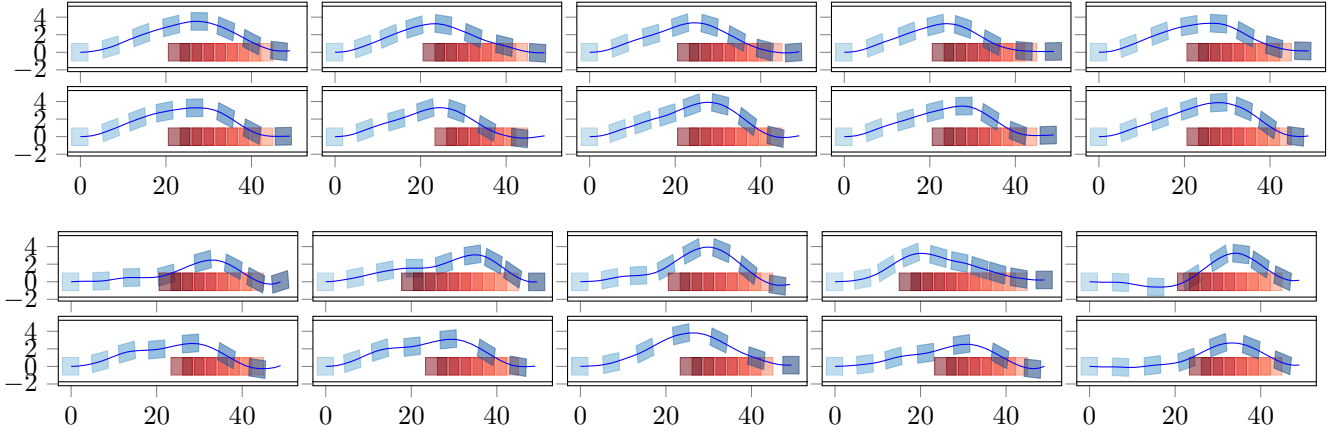


Fig. 5. Experiment 3. Trajectories for 10 different initial random seeds are displayed. The EV is driving from left to right, while the obstacle vehicle (red) is driving from right to left. (TOP 10) The case of implicitly considering the dynamic obstacle by setting an auxiliary setpoint in the neighboring lane to ensure obstacle avoidance. Obstacle points are only perceived from the static road bounds. (BOTTOM 10) The case of explicitly considering obstacle points of the dynamic obstacle. There are 4 obstacle points perceived from the obstacle vehicle and 16 from the road bounds. See Sect. III-C.

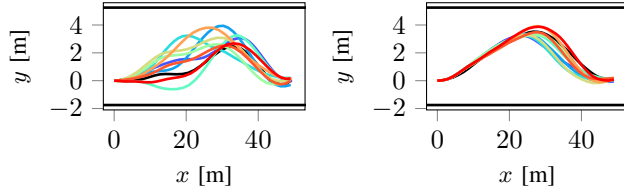


Fig. 6. Experiment 3. Trajectories for 10 different initial random seeds are displayed for (Left) explicitly accounting for the obstacle points of the dynamic obstacle vehicle vs. (Right) conducting obstacle avoidance via an auxiliary setpoint in the neighboring lane to implicitly account for the dynamic obstacle vehicle. Other quantifications are (Left) $\bar{\tau}_a = 0.090$ s and $v^{\min}/\bar{v}/v^{\max}=28.2/50.6/67.8$ km/h, and (Right) $\bar{\tau}_a = 0.085$ s and $v^{\min}/\bar{v}/v^{\max}=38.0/49.4/58.6$ km/h.

T_s	H	N_{restarts}	$N_{\text{iter}}^{\text{max}}$	n	N_{obstPts}
0.1	200	15	1	20480	20

ϵ_ξ	ϵ_η	ϵ_φ	ϵ_v	$\Delta\xi$	$\Delta\eta$	$\Delta\varphi$	Δv
1.0	0.25	$\frac{10\pi}{180}$	$\frac{5}{3.6}$	30	3.5	2π	$\frac{120}{3.6}$

TABLE II. All experiments use the same hyperparameters. All in SI-units.

TitanV-GPU. If plotted, the vehicle chassis is displayed every 0.5s and darker color (blue and red) means later in time. Throughout, standard multilayer perceptrons are used as NN-parametrization. For notation, NN-[5,2,2] denotes an input, hidden, and output layer of 5, 2, and 2 units, respectively.

A. Experiment 1: Characteristics of method in view of RRTs

The purpose of this experiment is to discuss a conceptual issue of RRTs that is not an issue for the proposed method. The experimental setup is $z_0 = [0, 0, 0, 0]$, $\zeta^{\text{goal}} = [0, 0, \pi, 0]$, no obstacle points and simulation over 10 different random seeds.

Suppose the RRT-algorithm [11] with a tree that is rooted at the origin z_0 . Suppose now that during the course of RRT-iterations at one point (Step 3 in Alg. of [11]) it is sampled $\zeta^{\text{goal}} = [0, 0, \pi, 0]$. Then the next question is what node in the tree to connect the sample to. The original RRT algorithm connects the sample to the “closest” node in the tree according to a *distance metric*. This “select nearest neighbor”-step (Step 4 in Alg. of [11]) is key to any RRT-

algorithm because it is responsible for the rapid expansion of the state space. However, at the same time it is also cause of controversy since it is in general not straightforward to decide what distance metric to use for that decision.

- 1) Suppose *Euclidean distance* is used as metric. Then, the root node z_0 would be closest and the 0-input would be requested (Step 5 in Alg. of [11]) for the transition from z_0 to the sample according to the Euclidean distance metric. Alternatively, when using the Euclidean distance only as metric for the nearest neighbor selection but not for the input selection (Step 5 in Alg. of [11]), then the original problem is recovered and any progress is prohibited by this looping. In both cases the mission is thus impossible to solve.
- 2) In [15] *Dubins path length* is used as distance metric. A Dubins path implies (i) constant forward speed, and (ii) to be at any time in either a maximal left-turning, straight or maximal right-turning motion. A Dubins path thus assumes it is possible to change instantaneously from maximal left-turn to maximal right-turn at any velocity. In view of RRT, there is consequently a *model mismatch* between the vehicle model used for the distance metric (Dubins car) and the actual vehicle model with (i) steering rate constraints and (ii) the capability to move both forward and reverse to connect any 2 vehicle poses.

An additional comment to RRT* [21] is made. The issue of distance metric selection perseveres also for RRT*. This is because it differs from the original RRT only in (i) the different method for parent node selection for a new sample, and (ii) in adding a step for rewiring tree connections based on cost (estimates) accounting for the new sample node.

This discussion is given to contrast simplicity and generality of the proposed method, which (i) does not involve any model mismatch at any stage (it is always worked with full vehicle dynamics and all of its constraints and motion capabilities), (ii) controls both steering and acceleration coupledly, and (iii) permits to sample unconstrainedly in the

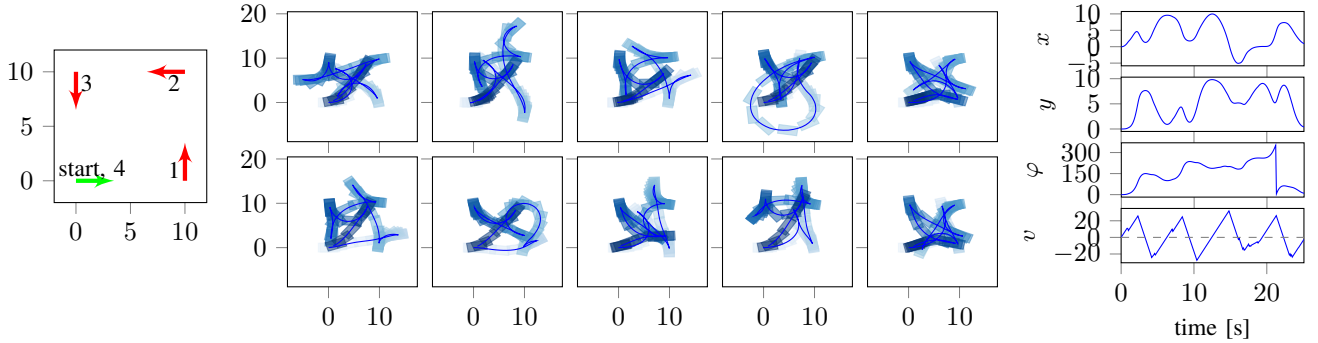


Fig. 7. Experiment 4. (Left) Mission formulation: 4 static waypoints (labeled 1-4) are meant to be tracked. (Center) Trajectories for 10 different initial random seeds. (Right) Vehicle states for the grid view at the top-left. Note that in all 10 cases all of the 4 waypoints are successfully tracked, requiring alternating forward and reverse motion and extensive steering. The influence of different random seeds and limited preview in closed-loop is clearly visible.

NN-architecture	$ \theta $	$ y ^{\max}$	$v^{\min}/\bar{v}/v^{\max}$	$\bar{\tau}_a$
[5, 2, 2]	18	0.51	33.5/50.4/64.9	0.036
[5, 10, 2]	82	0.29	28.0/46.0/65.0	0.047
[5, 10, 10, 2]	192	0.26	30.2/50.1/65.1	0.130
[5, 2, 2]†	18	0.32	37.9/51.6/63.5	0.036

TABLE III. Experiment 2. Two computation times are in bold for emphasis. The number of parameters for each NN is denoted by $|\theta|$. †: The experimental setup is identical, except that $\zeta^{\text{goal}}[0] = 25\text{m}$ is used instead of 50m as in the other cases.

parameter space of the NN, i.e., $\theta \in (-\infty, \infty)$, which is ideal for exploration, and (iv) the fact that controls $a_{t+h} = \mathcal{X}(s_{t+h}, \theta), \forall h = 0, \dots, H$, are varying over horizon H even for a small NN-[5,2,2] with only $|\theta| = 18$ parameters. Results for the experiment are displayed in Fig. 3. The influence of different initial random seeds is clearly visible (very different behaviors are obtained). Nevertheless, the mission is solved for all of them. Note that desirable 3-point steering is obtained in 9 out of 10 cases even though *no* auxiliary setpoints were set and 3-point-steering was thus not a priori encouraged in any form. Instead, it evolved naturally.

B. Experiment 2: Effect of NN-size

The experimental setup is $z_0 = [0, 0, 0, 50/3.6]$, $\zeta^{\text{goal}} = [50, 0, 0, 50/3.6]$, no obstacle points and simulation over 10 different random seeds. The objective is to analyze influence of NN-size on (i) average computation times $\bar{\tau}_a$ and (ii) on wiggling motion behavior characteristic for sampling based control. The latter is here measured by the maximal lateral overshoot $|y|^{\max}$ over all 10 simulations. Three NNs are compared: NN-[5,2,2], -[5,10,2] and -[5,10,10,2]. Results are summarized in Fig. 4 and Table III. The following trade-off is observed: the larger the NN the smaller $|y|^{\max}$, but the larger also $\bar{\tau}_a$. Maximal lateral overshoot could be reduced from 0.51m to 0.32m (while not compromising on $\bar{\tau}_a$) for the smallest NN-[5,2,2] by just reducing the initial distance of goal setpoint from 50m to 25m, see Table III. In all subsequent experiments NN-[5,2,2] is employed for its fastest computation times.

C. Experiment 3: Effect of obstacle points

The basic experimental setup is identical to Sect. III-B, however, (i) a dynamic obstacle moving *towards* the EV on the same lane at 20km/h starting at $x = 40$ which

must be avoided, and (ii) road-bounds at $y = -1.75\text{m}$ and 5.25m are added. The objective is (i) to monitor the effect of obstacle points on computation times, and (ii) to compare trajectories when (1) explicitly considering obstacle points of the dynamic obstacle vs. (2) implicitly considering the dynamic obstacle by setting an *auxiliary* setpoint in the neighboring lane and simultaneously discarding obstacle points of the dynamic obstacle. For this experiment, the total number of obstacle points² considered is $N_{\text{obstPts}} = 20$ in both scenarios. In the latter, all obstacle points are assigned to define road bounds. Results are displayed in Fig. 5 and 6. It is observed that (i) the inclusion of obstacle points causes an increase from $\bar{\tau}_a = 0.036\text{s}$ in the obstacle-free case of Experiment 2 to $\bar{\tau}_a = 0.090\text{s}$ here, and (ii) performing dynamic obstacle avoidance via an auxiliary setpoint generates more consistent and smoother motion over different random seeds. Since no velocity constraints were considered (to better observe sampling behavior), there are velocity variations as reported in the caption of Fig. 6. Note that velocity constraints can easily be enforced by discarding samples (i.e., NN-parametrizations) that violate these.

D. Experiment 4: Effect of randomization

The experimental setup is $z_0 = [0, 0, 0, 0]$, tracking of 4 static setpoints with position and heading as in Fig. 7, no obstacle points and simulation over 10 different random seeds. The objective is to analyze influence of randomization via different initial random seeds and to show capabilities of the method in a complex mission requiring extensive steering and alternating forward and reverse driving. Results are displayed in Fig. 7. For all 10 random seeds all 4 waypoints are successfully tracked. The influence of different random seeds is clearly visible (very different behaviors are obtained). More quantifications are: $\bar{\tau}_a = 0.035\text{s}$, $v^{\min}/\bar{v}/v^{\max} = -37.1/1.2/35.0\text{km/h}$ and $P^{\min}/\bar{P}/P^{\max} = 74/90/110\text{m}$.

E. Experiment 5: A reverse parking scenario

The experimental setup is $z_0 = [0, 2, 0, 0]$, simulation over 10 different random seeds, and tracking of 3 and 2 waypoints in a reverse parking-like scenario. In both cases,

²Each obstacle point is assumed as a 4D vector with planar location, heading and velocity information, see Sect. II-E.

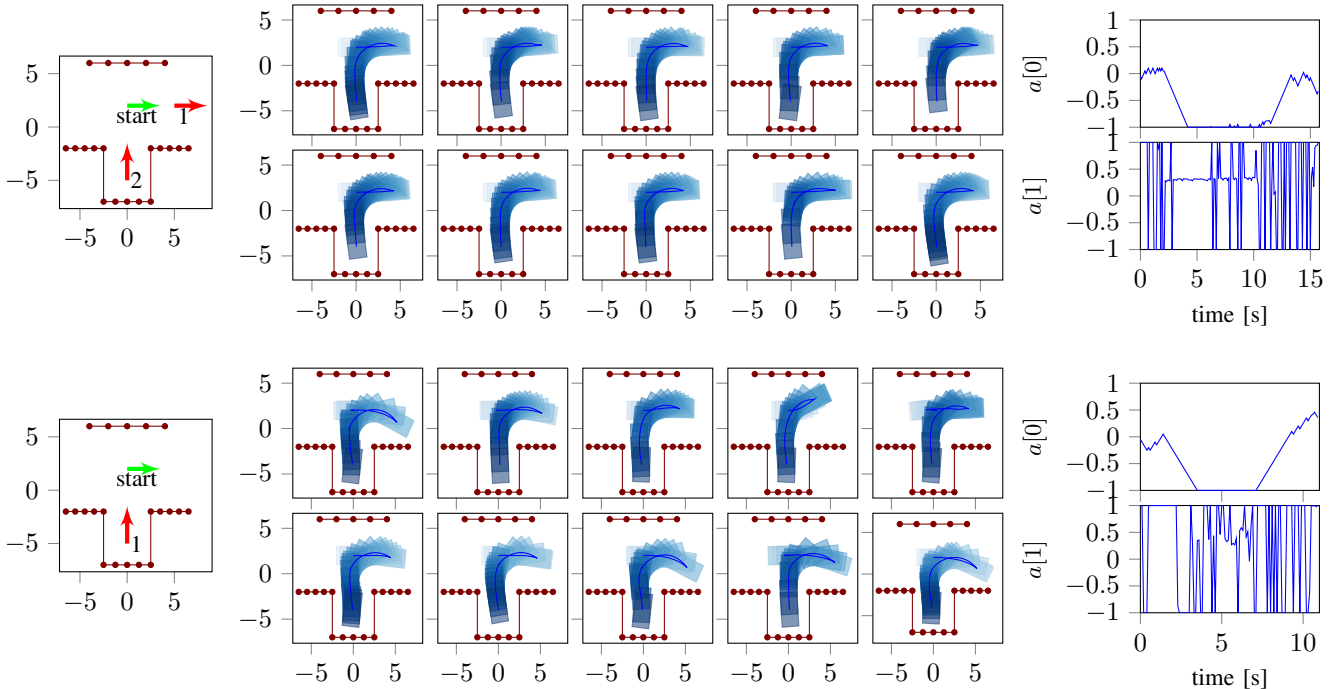


Fig. 8. Experiment 5. TOP ROW: (Left) Mission formulation: 3 static waypoints are tracked. These are “1”, an auxiliary one with $\zeta^{\text{goal}} = [0, 0, \pi/2, 0]$ (not displayed for clarity), and “2”. The static obstacle points are indicated by the dots. (Center) Trajectories for 10 different initial random seeds. (Right) Controls output from the NN-[5,2,2] for the grid view at the top-left. Note that the vehicle is operating at its handling limits (both absolute and maximum rate steering constraints are saturated). More quantifications averaged over all 10 random seeds are: $\bar{\tau}_a = 0.088\text{s}$, $v^{\text{min}}/\bar{v}/v^{\text{max}} = -17.3/-1.2/16.2\text{km/h}$ and $P^{\text{min}}/\bar{P}/P^{\text{max}} = 13.8/14.3/15.2\text{m}$. BOTTOM ROW: (Left) Mission formulation: 2 static waypoints are tracked. These are an auxiliary one (not displayed for clarity) with $\zeta^{\text{goal}} = [0, 0, \pi/2, 0]$ and “1”. (Center) Trajectories for 10 different initial random seeds. (Right) Controls output from the NN-[5,2,2] for the grid view at the top-left. Note that the vehicle is operating at its handling limits (both absolute and maximum rate steering constraints are saturated). More quantifications averaged over all 10 random seeds are: $\bar{\tau}_a = 0.088\text{s}$, $v^{\text{min}}/\bar{v}/v^{\text{max}} = -16.4/-1.5/19.1\text{km/h}$ and $P^{\text{min}}/\bar{P}/P^{\text{max}} = 12.5/15.7/17.8\text{m}$.

$N_{\text{obsPts}} = 20$ static obstacle points define the parking lot. The objective is to analyze influence of adding a suitable waypoint and to show capabilities of the method in a complex mission requiring extensive steering, alternating forward and reverse driving, and obstacle avoidance. Results are displayed in Fig. 8. In both cases for 3 and 2 waypoints, the mission is solved for all 10 random seeds. However, consistency of behavior is clearly improved when including a suitably selected third waypoint (“1” in the top row of Fig. 8).

IV. MORE COMMENTS

First, a beneficial characteristic of proposed method is that only a low-dimensional set of NN-parameters needs to be sampled at every T_s . Because of the NN-approach with, e.g., only $|\theta| = 18$ parameters for NN-[5,2,2], complex motion planning over long prediction horizons (e.g., $H = 200$) is still feasible. This is since while θ is held constant, the feature vector s_{t+h} is varying. Consequently also controls are varying with $a_{t+h} = \mathcal{X}(s_{t+h}, \theta)$, $\forall h = 0, \dots, H$.

Second, key hyperparameters were identified. Competing interests are on one hand large H , N_{restarts} , N_{obsPts} and large NNs, and on the other hand small computation times. Larger H are especially relevant for low-velocity navigation. For $H = 200$ and $T_s = 0.1\text{s}$ at $v = 5\text{km/h}$ the spatial look-ahead horizon is 27.8m. For perspective, in [10] $H = 4$ is used (for a 80km/h lane change). Note that $H = 4$ for $T_s = 0.1\text{s}$ at $v = 5\text{km/h}$ implies a spatial preview of only 0.56m. Larger N_{restarts} were found to improve

performance and be much more important than the $N_{\text{iter}}^{\text{max}}$ -iteration [19]. Therefore, $N_{\text{iter}}^{\text{max}} = 1$ in Table II. As illustrated in Table III, larger NN reduce wiggling, however increase computational time significantly. Likewise, considering many obstacle points significantly increases computation times. This is because at every $h = 0, \dots, H$ it has to be iterated over all obstacle points (first their motion extrapolation according to Sect. II-E, then collision checking). Heuristics to address this are (i) prefiltering of obstacle points deemed most relevant, and (ii) directing more research effort towards the online selection of goal setpoints ζ^{goal} . It was found in the experiments of Sect. III-C that motion was much less wiggly when performing dynamic obstacle avoidance by setting an auxiliary waypoint in the neighboring lane instead of explicitly accounting for the obstacle points of the dynamic obstacle.

Third, in general collision checking is considered to be the most expensive computational bottleneck in sampling-based motion planning algorithms [22]. The generality (arbitrary vehicle shapes, possibility to also account for shielded obstacle points, and expansion-possibility to 3D) and simplicity (linear inequality checks) of (2) comes at a cost, namely, the dependency on the resolution accuracy of finite N_{obsPts} obstacle points sufficiently characterizing all relevant obstacles.

Fourth, note that (eventhough on powerful hardware) all presented results were obtained *without* yet any guiding of the sampling distribution by heuristics [13], [23]. For

perspective, in [15, Sect. IV.A] sampling strategies heuristically vary for (i) on a lane, (ii) at an intersection, (iii) in parking lots, (iv) when passing a static obstacle, (v) for 3 different phases of a 3-point turn, and (vi) for reverse driving. Contrary to RRT-based methods, for warm-starting of proposed method it is not decisive *where* to sample spatially, but instead *what motion primitives* to offline pre-encode in the NN. This is because it is then on-top sampled online in the parameter space of the NN. Favorably, pre-encoding of motion primitives can simultaneously provide certificates about base performance. Such certificates may structurally be more valuable than aforementioned heuristics in [15, Sect. IV.A], which just *guide* the probabilistic sampling but do not actually provide equivalent certificates about performance.

Fifth, a main limitation of the current implementation of proposed method is that few obstacle points N_{obstPts} could be considered in simulations while maintaining a desired long prediction horizon H , a large number of restarts N_{restarts} , and remain within $T_s = 0.1\text{s}$. The considerations for ongoing work are therefore as follows: Since H must be maintained high to also admit a larger spatial preview at low velocities, two main tuning knobs remain to increase the computation time available for obstacle points collision checks. First, it is hoped that by pre-encoding of motion primitives for warm-starting the sampling efficiency is improved such that N_{restarts} can be reduced significantly, ideally, up to $N_{\text{restarts}} = 1$. Second, it is sought to develop, possibly geometric, mappings from mission data and obstacle points to good waypoints ζ^{goal} such that as many as possible obstacle points can be filtered out before feeding to the GPU for collision checking.

Ultimately, as Table III illustrated, smaller networks result in smaller computation times. The fact that a *small* NN-[5,2,2] with only $|\theta| = 18$ parameters could solve all of above 5 experiments is a very promising sign for future work merging proposed online sampling with offline pre-encoding. This is since in [20] it was found that tiny NNs are sufficient to offline encode many motion primitives.

V. CONCLUSION

A simple method for online sampling in the parameter space of a neural network for GPU-accelerated motion planning of autonomous vehicles was proposed. It is designed for parallelization and therefore well-suited to benefit from continuing advancements in hardware such as GPUs.

There are 2 main avenues for future work. First, preliminary offline encoding of motion primitives in the NN is considered in order to obtain a better warm-start initialization for on-top online sampling, and to obtain (offline-generated) certificates about base performance. This preliminary offline encoding is expected to accelerate online sampling through better guided randomization. In general, sampling in the parameter space of a NN for control seems particularly promising since NNs are a natural choice for offline pre-encoding of motion primitives. Second, methods for efficient online waypoint selection (guided by traffic rules and geometric consideration) must be devised, possibly also as a function of offline pre-encoded motion primitives to guarantee specific performance.

REFERENCES

- [1] D. González, J. Pérez, V. Milanés, and F. Nashashibi, "A review of motion planning techniques for automated vehicles," *IEEE Trans. on Intelligent Transport. Systems*, vol. 17, no. 4, pp. 1135–1145, 2016.
- [2] J. H. Reif, "Complexity of the mover's problem and generalizations," in *IEEE Annual Symposium on Foundations of Computer Science*, pp. 421–427, 1979.
- [3] T. Lozano-Pérez and M. A. Wesley, "An algorithm for planning collision-free paths among polyhedral obstacles," *Communications of the ACM*, vol. 22, no. 10, pp. 560–570, 1979.
- [4] M. Brown, J. Funke, S. Erlien, and J. C. Gerdes, "Safe driving envelopes for path tracking in autonomous vehicles," *Control Engineering Practice*, vol. 61, pp. 307–316, 2017.
- [5] H. Andersen, W. Schwarting, F. Naser, Y. H. Eng, M. H. Ang, D. Rus, and J. Alonso-Mora, "Trajectory optimization for autonomous overtaking with visibility maximization," in *IEEE International Conference on Intelligent Transportation Systems*, pp. 1–8, 2017.
- [6] M. G. Plessen, D. Bernardini, H. Esen, and A. Bemporad, "Spatial-based predictive control and geometric corridor planning for adaptive cruise control coupled with obstacle avoidance," *IEEE Transactions on Control Systems Technology*, vol. 26, no. 1, pp. 38–50, 2018.
- [7] K. Oyama and K. Nonaka, "Model predictive parking control for non-holonomic vehicles using time-state control form," in *IEEE European Control Conference*, pp. 458–465, 2013.
- [8] B. Li, Y. Zhang, F. Dou, and Y. Liu, "Real-time trajectory planning for agv in the presence of moving obstacles: A first-search-then-optimization approach," *arXiv preprint arXiv:1902.06201*, 2019.
- [9] M. Hamer, L. Widmer, and R. D'Andrea, "Fast generation of collision-free trajectories for robot swarms using gpu acceleration," *IEEE Access*, vol. 7, pp. 6679–6690, 2019.
- [10] K. Berntorp, "Path planning and integrated collision avoidance for autonomous vehicles," in *American Control Conference*, pp. 4023–4028, 2017.
- [11] S. M. LaValle, "Rapidly-exploring random trees: A new tool for path planning," 1998.
- [12] J. J. Kuffner Jr and S. M. LaValle, "RRT-connect: An efficient approach to single-query path planning," in *IEEE International Conference on Robotics and Automation*, vol. 2, 2000.
- [13] C. Urmsen and R. Simmons, "Approaches for heuristically biasing RRT growth," in *IEEE/RSJ International Conference on Intelligent Robots and Systems*, vol. 2, pp. 1178–1183, 2003.
- [14] D. Ferguson, N. Kalra, and A. Stentz, "Replanning with RRTs," in *IEEE International Conference on Robotics and Automation*, pp. 1243–1248, 2006.
- [15] Y. Kuwata, J. Teo, G. Fiore, S. Karaman, E. Frazzoli, and J. P. How, "Real-time motion planning with applications to autonomous urban driving," *IEEE Transactions on Control Systems Technology*, vol. 17, no. 5, pp. 1105–1118, 2009.
- [16] J. Bialkowski, S. Karaman, and E. Frazzoli, "Massively parallelizing the RRT and the RRT*," in *IEEE/RSJ International Conference on Intelligent Robots and Systems*, pp. 3513–3518, 2011.
- [17] D. Dolgov, S. Thrun, M. Montemerlo, and J. Diebel, "Path planning for autonomous vehicles in unknown semi-structured environments," *The International Journal of Robotics Research*, vol. 29, no. 5, pp. 485–501, 2010.
- [18] B. Paden, M. Čáp, S. Z. Yong, D. Yershov, and E. Frazzoli, "A survey of motion planning and control techniques for self-driving urban vehicles," *IEEE Transactions on Intelligent Vehicles*, vol. 1, no. 1, pp. 33–55, 2016.
- [19] M. G. Plessen, "Automating vehicles by deep reinforcement learning using task separation with hill climbing," in *Future of Information and Communication Conference*, pp. 188–210, Springer, 2019.
- [20] M. G. Plessen, "Encoding motion primitives for autonomous vehicles using virtual velocity constraints and neural network scheduling," in *IEEE International Conference on Machine Learning and Applications*, pp. 208–215, 2018.
- [21] S. Karaman, M. R. Walter, A. Perez, E. Frazzoli, and S. Teller, "Anytime motion planning using the RRT*," in *IEEE International Conference on Robotics and Automation*, pp. 1478–1483, 2011.
- [22] J. Bialkowski, M. Otte, S. Karaman, and E. Frazzoli, "Efficient collision checking in sampling-based motion planning via safety certificates," *The International Journal of Robotics Research*, vol. 35, no. 7, pp. 767–796, 2016.
- [23] B. Ichter, J. Harrison, and M. Pavone, "Learning sampling distributions for robot motion planning," in *IEEE International Conference on Robotics and Automation*, pp. 7087–7094, 2018.